HEFAT2011
8th International Conference on Heat Transfer, Fluid Mechanics and Thermodynamics
11 – 13 July 2011
Pointe Aux Piments, Mauritius

GAS HEATING IN PLASMA MICROCAVITIES: SURFACE EFFECTS

M. Jugroot
Department of Mechanical and Aerospace Engineering
Royal Military College of Canada
Kingston, Ontario, K7K 7B4
Canada
E-mail: jugroot-m@rmc.ca

ABSTRACT

Interest in microcavities containing plasmas is growing rapidly due to the number of high-technology applications: such as active flow control, spacecraft propulsion, controlled combustion and pollution control. The present paper discusses a self-consistent model for gas and charged and species dynamics in atmospheric microcavities. A self-consistent and time-dependant model is described and applied with emphasis on terms involved in the close coupling among the fluid, the charged species and the electric field. The microplasmas are studied from an initial cloud until the stages of charged particle over-amplification and breakdown in small-spaces, where transients are particularly important. The importance of surface effects (namely secondary emission of charged particles from the electrodes) is compared in terms of spatial and temporal evolution of the plasma and fluid dynamics. Heating effects and gas depletion initiation are observed, highlighting the close interaction between neutral gas and charged species in governing the evolution of the microplasma.

INTRODUCTION

Microcavities and microplasmas are very interesting for miniaturization of devices for use in microelectro-mechanical systems, such as spectrometers, advanced flow control and advanced spacecraft propulsion systems [1-4]. Microplasmas have unique features and more modeling and plasma diagnostics are needed to identify phenomena specific to microdischarges. Interestingly, from the physical point of view, short-gaps are short along both the interelectrode separation as well as boundary wall distance, thus leading to a characteristic behavior in the spatio-temporal evolution of the discharge. There are numerous unresolved questions to elucidate in order to better understand the phenomena involved in microplasmas where complex behaviors are observed [5-6] (for example fluid heating). For instance, concerning the surface effect responsible for the maintain of the discharge, the question of electronic secondary emission at the cathode appears as a very important one. Indeed, the primary electron swarm is rapidly absorbed after a brief transit time in the inter-electrode distance. Hence, the efficiency of the secondary emission plays an important role in both the maintain of the discharge and the different transitions. The question of surface effects becomes even more critical to capture when different electrode materials are used. In the present study, different emission coefficients representing different materials are discussed in terms of particle amplification and fluid dynamics. Furthermore, in small-space discharges, the energy transfer to the neutral gas as a result of collisions between charged and neutral particles, induces energy gradients and can in turn induce a convective movement of neutral particles. The flow pattern and profile of the neutral gas are believed to be significantly different in the small geometries as compared to larger configurations. Interestingly enough, this gas heating and convective motion of neutrals can initiate heterogeneity of the neutral density *N*. Gas heating and fluid dynamics are therefore important considerations in understanding and optimizing electrical properties of micro-devices [7]. The formalism described puts forward a global approach (fluid and plasma dynamics) in the numerical modeling of microcavities/microplasmas.

NUMERICAL METHOD

The neutral dynamics is governed by the macroscopic hydrodynamic equations of a compressible and viscous fluid comprising conservation equations of densities of mass $m_N N(\vec{r},t)$, momentum $m_N N(\vec{r},t)\vec{v}_N(\vec{r},t)$ and total energy $\varepsilon(\vec{r},t)$ respectively:

$$\frac{\partial m_N N(\vec{r},t)}{\partial t} + \nabla_{\vec{r}}[m_N N(\vec{r},t)\vec{v}_N(\vec{r},t)] = 0, \qquad (1)$$

$$\frac{\partial m_N N(\vec{r},t)\vec{v}_N(\vec{r},t)}{\partial t} + \nabla_{\vec{r}}[m_N N(\vec{r},t)\vec{v}_N(\vec{r},t)\vec{v}_N(\vec{r},t)] =$$

$$n_s \frac{m_N m_s}{(m_N + m_s)} \upsilon_{sN}(\vec{v}_s - \vec{v}_N) \; - \nabla_{\vec{r}} p \overset{\Rightarrow}{I} - \nabla_{\vec{r}} \overset{\Rightarrow}{\tau}, \qquad (2)$$

$$\frac{\partial \varepsilon(\vec{r},t)}{\partial t} + \nabla_{\vec{r}}[\varepsilon(\vec{r},t)\vec{v}_N(\vec{r},t)] =$$

$$\nabla_{\vec{r}} Q - \nabla_{\vec{r}}[\vec{v}_N.(p \overset{\Rightarrow}{I} + \overset{\Rightarrow}{\tau})] + f_t \vec{J}.\vec{E} \qquad (3)$$

$m_N, N(\vec{r},t), v_N(\vec{r},t), p$ and T are the mass, density, velocity, pressure and temperature of the gas respectively. $\vec{r}$ and t represent the vector position and time. υ_{sN} is the collision frequency between charged and neutral particles, ε total energy; k_B is the Boltzmann constant and $\overset{\Rightarrow}{I}$ is the identity tensor. The system of transport equations 1 to 3 is closed by the equation of state of an ideal gas ($p=k_BNT$) and by Fourier's law for the heat flux Q and the Newtonian approximation for the viscous tensor $\overset{\Rightarrow}{\tau}$.

Note that the three equations describing the neutral dynamics are not only strongly coupled but are moreover dependent on the charged particles dynamics via the terms $n_s \frac{m_N m_s}{(m_N + m_s)} \upsilon_{sN}(\vec{v}_s - \vec{v}_N)$ and $f_t \vec{J}.\vec{E}$. Indeed, these terms represent respectively the action of the plasma on the neutral gas by two modes of transfer namely momentum (due to convection) and energy transfer (due to Joule heating). This implies that the neutral dynamics is conditioned by the charged particle dynamics which can be represented by the conservation equations for charged particles. Equation 4 shows the conservation equation for charged species (*s*: electrons and ions respectively, for the plus and minus signs in second RHS term). For ions, the drift-diffusion formulation was also compared to the ion momentum equation in our simulations and results were found to be very similar. Equation 5 depicts the Poisson equation describing the potential *V* and the corresponding electric field *E*, including space charge effects:

$$\frac{\partial n_s}{\partial t} + \nabla_{\vec{r}}\{\pm n_s \mu_s N \frac{\vec{E}}{N} - D_s \nabla_{\vec{r}}[n_s]\} = S_s, \qquad (4)$$

$$\Delta V = -\frac{\rho}{\varepsilon_0} = -\frac{e(n_i - n_e)}{\varepsilon_0} \quad \text{with } \vec{E} = -\nabla_{\vec{r}} V \qquad (5)$$

The subscript s refers to the particle considered, n_s is the density (n_e and n_i are electron and positive ion densities), $\vec{v}_s$ the mean velocity, S_s the source term, D_s the diffusion coefficient, μ_s the mobility and *e* the electron charge.

The simulations are undertaken in two dimensional Cartesian coordinates, in the case of plane parallel metallic and dielectric electrode configurations. There is no outside flow in the confined microcavity. The inter-electrode distance (*y*-direction) is 200 μm and the transverse dimension (*x*-direction) of the simulation domain is about 5.2 mm. The discharge is initiated by releasing an electron swarm near the cathode and the evolution is followed till the stage of particle over-amplification.

The discharge is maintained by secondary emission and amplified by ionization processes (direct, stepwise and Penning (of impurities) ionizations are considered). Under these conditions, the source term of Eq. (4) can be written as:

$$S_e = S_i = \nu_{ion} n_e + k_{em} n_e n_m + k_{pm} n_m n_p . \qquad (6)$$

The first right hand side term represents direct ionization, the second term stepwise ionization, and the third is due to Penning ionization. k_{pm} is a rate coefficient approximated to 5 10^{-10} cm^{-3} s^{-1}, n_p the density of impurities roughly estimated to a relative density of 10^{-4} corresponding to 2.5 10^{15} cm^{-3}. Thus, in helium it is necessary to add a further equation to account for the evolution of metastable density n_m:

$$\frac{\partial n_m}{\partial t} - D_m \nabla_{\vec{r}} n_m = \nu_{ex} n_e - k_{em} n_e n_m - k_{pm} n_m n_p . \qquad (7)$$

ν_{ex} represents the electron-atom excitation frequency. The boundary conditions on the metallic electrodes for particles are classical [8] (for instance $\partial n_e / \partial y = 0$ and $n_i = n_m = 0$ at the anode; and $n_m = 0$ and $\partial n_i / \partial y = 0$ at the cathode, *x* and *y* being the transverse and longitudinal directions with respect to the direction of the applied electric field).

The electron distribution at the cathode in the helium microplasma is determined by assuming that the total flux from the cathode $n_{ec} v_e$ is equal to the total density of the cathode emission frequency:

$$n_{ec} v_e = \gamma_i n_i v_i + \gamma_m n_m v_m + \gamma_{ph} \upsilon_{ph} . \qquad (8)$$

$n_i v_i = \mu_i n_i E$ is the ion flux from the cathode and $n_m v_m = -D_m (\partial n_m / dy)$ is the metastable flux. Secondary emission has been shown to be a critical parameter in microplasmas and two values are discussed in the present paper. Several modes of secondary emission (such as photoemission and field emission – as field emission may also play a role in microcavites) were investigated and compared for a short-gap hydrogen discharge [5].

Concerning the boundary conditions for the gas species, the electrodes are considered to be cold except in the plasma region where the temperature rises locally due to Joule effects. These thermal effects do not have time to propagate in the electrodes as the lifetime of the discharge is not long enough. Following the viscous fluid approximation, the conditions on the electrodes are treated so as to encompass boundary layer assumptions. Hence the velocity field tends to flow parallel near the electrodes and is nil on the electrodes and thermal

accommodation is used for temperature conditions for the gas very close to the electrodes.

The equations are discretized by the method of finite control volume with the approximation of centered difference at the frontiers and solved by the flux corrected transport (FCT) algorithm [9]. In order to consider both transverse and longitudinal directions, a time-splitting approximation has been used in the FCT algorithm. The Poisson equation is solved by an efficient Fast Fourier Transform (FFT) algorithm following both *x* and *y* directions.

RESULTS AND DISCUSSION

The primary objective is to compare differences in general behavior for microcavities with different secondary emission properties at the electrodes and its impact on fluid and charged species dynamics. A helium microcavity (200 μm) at atmospheric pressure and at 293 K with an applied dc voltage of 449 V is investigated. The microcavity is occluded and does not contain any gas flow. The primary electron swarm is exposed to a strong convective effect and begins to move towards the anode, which is reached after a few nanoseconds, while the ions are slowly attracted towards the cathode. The primary electrons are thus rapidly absorbed and the discharge is sustained by the secondary emission at the cathode.

For both cases of secondary emission investigated, the trends are similar as discussed hereafter. The density profiles do not change significantly during the first amplification phase during which spatial gradients are conserved, implying more uniform discharge characteristics (exponential longitudinal growth, nearly constant temporal growth rate and transverse population profiles close to Gaussian shape). During the first period, the ion space charge gradually builds up as a consequence of the relatively small ion mobility compared to the electronic mobility. The corresponding electric field is equal to the applied electric field at that point.

The next sequence is subsequently governed by the strong electric field induced by the space charge. As a matter of fact, the electric field increases due to the excess of ionic species compared to electronic ones. The onset of space charge effects can be seen for example at 54 ns (Figure 1). The differences in ion and electron densities lead to a strong local electric field which is conserved and builds up continuously as the net charge increases. Figure 1 gives a clear description of the evolution of charged particle dynamics. The figures also clearly show that the discharge dynamics is governed by the gradually increasing space charge. Interestingly enough, the distortion of the electric field in the anode half of the inter-electrode spacing decreases not only the ionization frequency in the anode region but also the electron and ion velocities, while near the cathode the enhancement of the electric field causes opposite effects. Hence, a rapid accumulation of electrons is observed in mid-gap region, for instance at t=54 ns (Figure 1).

This accumulation in turn enhances ionization processes, and thereby increases the ion density as electrons are rapidly evacuated to the anode due to the strength of the electric field. Consequently, the electric field is further increased, thus reinforcing the whole process previously described. This leads to a self amplification effect illustrated at t=58 ns in Furthermore, it can be observed that during the evolution, the accumulation or reinforced ionization moves progressively towards the cathode. This effect happens as a result of a competition between ionization and transport effects, as amplification due to ionization becomes progressively preponderant with respect to the electron transport). In fact, the cathode zone (region close to the cathode) is initiated by the combined effects of strong electron mobility and an insufficient electronic flux from secondary emission. The same trends are observed for both values of secondary emission (γ=0.05 and 0.1) investigated. However, due to the fact that fewer electrons are produced at the cathode in order to compensate for the losses, the amplification and associated effects are reduced and occur at a later time.

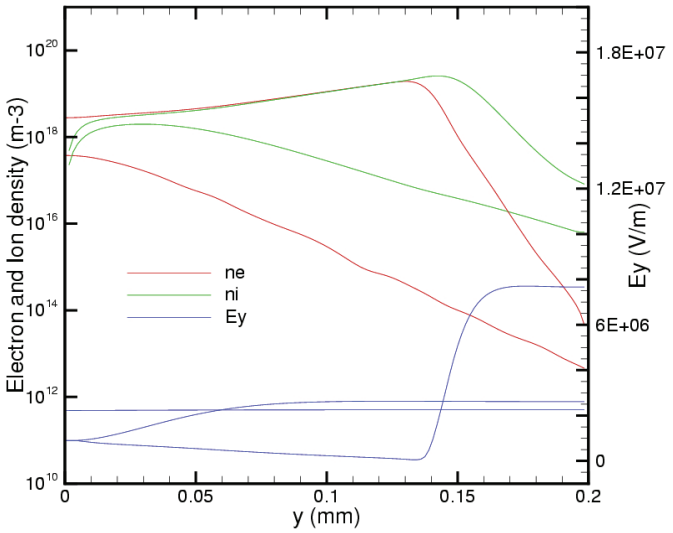

Figure 1 Electron (red), ion density (green) and longitudinal electric field (blue) at t=54 and 58 ns in helium. Potential applied is 449 V; Secondary emission coefficient is 0.05; the anode y=0 mm and cathode y= 0.2 mm.

The electric field profile allows an increasing number of electrons to be generated by secondary emission, but is overall insufficient to compensate for the lack of electrons in the cathode fall region. As a consequence of the electric field distribution and related particle amplification, a classical structure consisting of three distinct parts (cathode region, a positive column and anodic zone) [10] is observed. Fairly distinct anode and cathode sheaths are observed, the latter being significantly larger. The multidimensional structure of the discharge is depicted in Figure 2 and dimensions of the computational domain are also indicated. The figure shows the accumulation of electrons close to the cathode.

The charged particle distribution and amplification observed and described above are to a great extent specific to small-gaps as the electrons drift very rapidly across and are readily absorbed. This rapid absorption and subsequent amplification have been shown to in turn modify the global

charged particle dynamics as well as the neutral gas described hereafter.

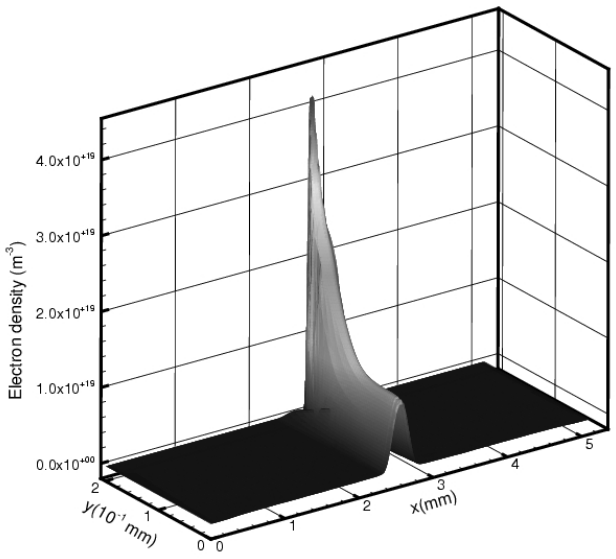

Figure 2 Electron density showing structure of discharge; Potential applied is 449 V; Secondary emission coefficient is 0.1; anode at y=0 mm and cathode at y= 0.2 mm.

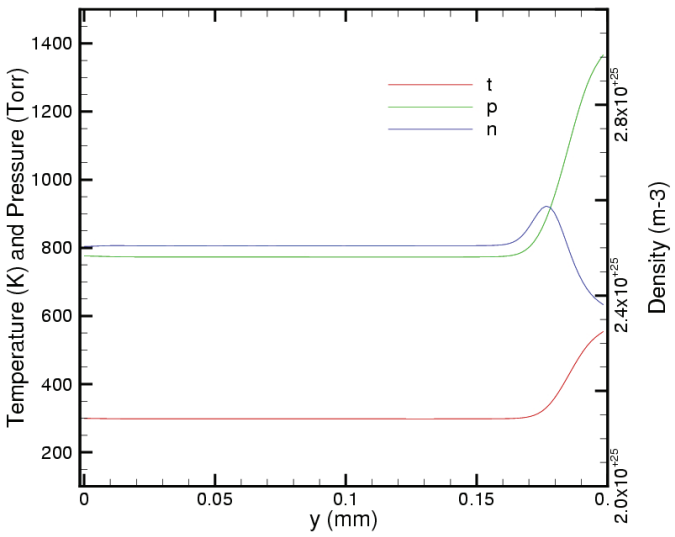

Figure 3 Distribution of gas pressure, temperature and density for t=70 ns along the discharge axis. Potential applied is 449 V; Secondary emission coefficient is 0.05; anode at y=0 mm and cathode at y= 0.2 mm.

The charged species distributions and electric field profile also contribute significantly to gas heating in the microplasma. As a matter of fact, in our case the Joule heating effect becomes very important for the 449 V case and a rise of the gas temperature is clearly observed in the cathode region of the microplasma. The gas heating peaks near the cathode and this trend is consistent with experimental observations. The temperature of the neutral gas rises to 550 K in the cathode region. An initiation of rarefaction of the neutral gas is also observed (Figure 3). The accumulation of energy and momentum effects creates a high pressure zone, 1400 torr, near the cathode. This energy and momentum accumulation triggers the movement of the neutral gas and induces a neutral depopulation. In fact, the neutral gas dynamics is mainly controlled by the Joule heating term due to collisions between charged particles (accelerated under the electric field) and neutral particles, as taken into account in the present self-consistent model. The magnitude of the Joule heating term is high enough to induce significant gas heating and to initiate neutral gas depletion near the cathode. The gas heating and neutral depletion effects are evident at the initial stages of the breakdown. The depletion effect will in turn affect the subsequent evolution of the microplasma. The heat transfer at the surface will be investigated in future work. Interestingly enough, the heating is fairly localized and can be possibly controlled by alternating metallic and dielectric electrode materials for high-technology applications such as in active flow control systems.

CONCLUSION

The charged particle distribution and amplification observed in this study are to a great extent specific to small gaps as the electrons drift very rapidly across and are readily absorbed. We have shown several phases in the evolution of helium microplasmas initiated by an electronic swarm and maintained by secondary emission and ionization. The fluid-plasma self-consistent formalism implemented in the present model clearly shows the prime importance of coupled effects in microcavities. Hence, this interdependence is clearly highlighted by space charge effects and neutral heating leading to the initiation of gas depletion. The differences between different secondary emission coefficients for electrodes have been discussed. The distribution of the species of the plasma is different but the same global features are observed. In all cases investigated, both charged and neutral effects characterize and govern the evolution of the microplasmas. We are currently applying self-consistent modeling to investigate the physical behavior in microdischarges designed for miniaturized systems such as micropropulsion devices and active flow control.

REFERENCES

[1] J. Hopwood and Y. Minayeva, *J. Vac. Sci. Techol. B* **18**, (2005)
[2] K.H. Becker, J.G. Eden and K.H. Schoenbach, *J. Phys. D: Appl. Phys.*, **38**, R357 (2005)
[3] I.D. Boyd, *Progress in Aerospace Sciences* **41**, 669 (2005)
[4] M. Jugroot, C.P.T. Groth, B. Collings, V. Baranov, B. Thomson and J.B. French, *J. Phys. D: Appl. Phys.* **41**, 025205 (2008)
[5] M. Jugroot, P. Bayle, M. Yousfi and O. Eichwald, *J. Phys. D: Appl. Phys.* **32**, 106 (1999)
[6] M. Jugroot, *Plasma Process. Polym.* **6**, (2009)
[7] M. Kushner, *J. Phys. D: Appl. Phys.* **38**, 1633 (2005)
[8] J.P. Novak and R. Bartnikas, *J. Appl. Phys.* **64**, 1767 (1988)
[9] J.P. Boris and D.L. Book, *J. Comput. Phys.* **135**, 172 (1997)
[10] T. Farouk, B. Farouk, A. Gutsol and A. Fridman, *J. Phys. D: Appl. Phys.,* **41**, 4175202 (2008)